



# Fabrication of porous carbon nanofibers with adjustable pore sizes as electrodes for supercapacitors

Chau Tran, Vibha Kalra\*

3141 Chestnut St, Department of Chemical and Biological Engineering, Drexel University, Philadelphia, PA 19104, USA

## HIGHLIGHTS

- Fabrication of free-standing porous carbon nanofibers (CNFs) using electrospinning.
- We demonstrate interconnected pore structure inside carbon nanofibers using TEM.
- Porous CNFs exhibit  $1600 \text{ m}^2 \text{ g}^{-1}$  specific surface with large fraction of mesopores.
- Porous CNFs exhibit  $210 \text{ F g}^{-1}$  at  $1 \text{ A g}^{-1}$  current and retain 75% capacitance at  $20 \text{ A g}^{-1}$ .
- Porous CNFs exhibit high power due to hierarchical pore structure.

## ARTICLE INFO

### Article history:

Received 4 September 2012

Received in revised form

11 January 2013

Accepted 15 January 2013

Available online 6 February 2013

### Keywords:

Electrical double layer supercapacitors

Porous carbon nanofibers

Electrospinning

Nafion

Cyclic voltammetry

Transmission electron microscopy

## ABSTRACT

We report a facile method for obtaining extremely high surface area and uniformly porous carbon nanofibers for supercapacitors. Blends of polyacrylonitrile and sacrificial Nafion at different compositions have been electrospun into non-woven nanofiber mats with diameters in the range of 200–400 nm. Electrospun nanofiber mats are then subjected to carbonization to obtain porous carbon nanofibers (CNFs) as polyacrylonitrile converts to carbon and Nafion decomposes out creating intra-fiber pores. Resultant porous CNFs exhibit specific surface area of up to  $1600 \text{ m}^2 \text{ g}^{-1}$  with a large fraction of mesopores (2–4 nm). No additional chemical or physical activation process was used. We demonstrate the tunability of the pore sizes within CNFs by varying the amount of Nafion. The non-woven fiber mats of porous CNFs are studied as free-standing electrode materials for supercapacitors eliminating the need for polymeric binding agents. Electrochemical measurements showed large specific gravimetric and volumetric capacitances of up to  $210 \text{ F g}^{-1}$  and  $60 \text{ F cm}^{-3}$  in  $1 \text{ M H}_2\text{SO}_4$  at a high cyclic voltammetry scan rate of  $100 \text{ mV s}^{-1}$  due to the large fraction of mesopores. These materials retain 75% performance at a large current density of  $20 \text{ A g}^{-1}$  indicating excellent power handling capability.

© 2013 Elsevier B.V. All rights reserved.

## 1. Introduction

Electrochemical double layer capacitors (EDLCs, also called supercapacitors or ultracapacitors) are one of the most promising energy storage devices owing to their high power density, rapid charging/discharging ability, and long cycle life. Their applications can range from low power mobile devices to high power electric vehicles. The basic operating principle involves the adsorption and desorption of ions at the electrode/electrolyte interface. The key factors that govern the capacitance or performance of these devices are the specific surface area and electrical conductivity of the electrode materials [1]. Porous carbon has been subjected to intensive

studies for supercapacitor applications because of its chemical and thermal stability, high conductivity, and relatively low cost. A wide range of porous carbons, such as activated carbon [2–4], carbide-derived carbon [5], carbon onions [6], carbon nanotubes [7], carbon aerogel [8,9], templated carbon [10], and carbon nanofibers [11–13] have been synthesized. These carbonaceous materials exist in various forms, such as powders, monoliths, thin films, fibers, and papers. Among them, carbon papers or fiber mats (woven or non-woven) have a lot of advantages since they can be fabricated into free-standing electrode materials without the addition of polymeric binding agents that are known to add dead mass and reduce the overall specific capacitance and conductivity of the electrodes.

Electrospinning is a simple process for fabricating non-woven nanofiber mats with high surface area and porosity. A typical electrospinning setup consists of a metallic spinneret, a syringe pump, a high-voltage power supply, and a grounded collector in

\* Corresponding author. Tel.: +1 215 895 2233; fax: +1 215 895 5837.

E-mail address: [vk99@drexel.edu](mailto:vk99@drexel.edu) (V. Kalra).

a humidity controlled chamber. A polymer solution, polymer melt or a sol–gel solution is continuously pumped through the spinneret at a constant rate, while a high-voltage gradient is applied between the spinneret tip and the collector substrate. The solvent continuously and rapidly evaporates while the jet stream is whipped and stretched by electrostatic repulsion forming solidified continuous nanofibers (diameters  $\sim 50$ – $500$  nm) on the grounded collector. Carbon nanofiber (CNF) mats can be fabricated by subjecting electrospun nanofibers of an appropriate polymer precursor to stabilization and carbonization processes. Cellulose, phenolic resins, polyacrylonitrile (PAN), polybenzimidazol, and pitch-based materials have been electrospun to produce CNFs. Among them, PAN is widely used as a precursor for CNFs due to its excellent electrospinnability and relatively high carbon yield. So far CNFs produced from electrospinning PAN have been subjected to different physical or chemical activation processes using steam [14],  $\text{CO}_2$  [15], or  $\text{NaOH}$  [16] to create pores within nanofibers. The activation process further increases the specific surface area of carbon nanofibers thereby enhancing the specific capacitance. However, these activation processes often create micropores that are less than 2 nm in diameter and provide little control over pore sizes and overall porosity within nanofibers. These materials often show a big drop in capacitance when used in non-aqueous, organic electrolytes and/or at high current densities [16], conditions that are necessary for most industrial/practical applications. Moreover, the activation step can modify the surface functionalities of CNFs which results in cycling instability of supercapacitors [17].

Some researchers have electrospun blends of PAN with other sacrificial polymers to generate a range of phase-separated structures in the fibers. The overall idea was that upon carbonizing at high temperature, PAN will convert to carbon, and the sacrificial polymer would be decomposed out to create intra-fiber pores. The concept is very interesting and potentially powerful since the need for activation will be eliminated and the number of steps to produce porous CNFs will be reduced; however, so far not much success in terms of obtaining high surface areas as well as uniform distribution of intra-fiber pores has been seen. Ji et al. [18] prepared porous CNFs by carbonizing electrospun PAN/poly(L-lactide) nanofibers. They obtained irregular thin long interior pores within carbon nanofibers and a specific surface area of  $359 \text{ m}^2 \text{ g}^{-1}$ . Given that pure PAN-derived non-porous carbon nanofibers have been shown to exhibit a specific area of up to  $240 \text{ m}^2 \text{ g}^{-1}$  [19], little advantage of the presence of a sacrificial polymer was demonstrated. Zhang and Hsieh [20] electrospun binary solutions of PAN with three different sacrificial polymers, poly(ethylene oxide), cellulose acetate, and poly(methyl methacrylate) (PMMA). Upon removal of the second polymer and subsequent carbonization, different features such as grooved, hollow, U-shaped, or collapsed fibers were observed, and there was no report of specific surface area. Similarly, porous CNFs with hollow cores were obtained by electrospinning PAN and PMMA by Kim et al. [21]. The carbonized samples exhibited a high surface area of  $940 \text{ m}^2 \text{ g}^{-1}$ , however the paper focused largely on material synthesis and no study on utilizing this material for energy application was reported. Niu et al. [22] produced bonded CNFs by carbonizing nanofibers containing PAN and thermoplastic polyvinylpyrrolidone. However, structure within nanofibers was not reported. Recently, other researchers also electrospun PAN with catalyst materials such as  $\text{ZnCl}_2$  or polymethylhydrosiloxane to create pores on the outer surface of CNFs. The resultant porous CNFs contained a majority of micropores with a specific surface area of up to  $550 \text{ m}^2 \text{ g}^{-1}$  and a specific capacitance of up to  $160 \text{ F g}^{-1}$  in 6 M KOH [19,23].

In this work, we provide a facile route to fabrication of porous carbon nanofibers (CNFs) with uniformly distributed pores within the nanofibers via electrospinning. A binary mixture of PAN and a rigid mechanically stable polymer, Nafion in dimethylformamide

(DMF) was electrospun into non-woven nanofiber mats. Our previous work [24] indicated that the rapid solvent evaporation and short residence time during electrospinning limits the available phase separation time resulting in the formation of co-continuous assembly of PAN and Nafion with a nanoscale domain size inside the nanofibers. After stabilization and carbonization, as shown in this paper, the Nafion domains were decomposed, and the residual PAN domains were converted to carbon with an interconnected pore network throughout the entire fibers. Unlike other sacrificial polymers studied in the past, Nafion was used to create pores because of its rigidity and high decomposition temperature. This in turn prevented fibers from shrinking and collapsing during stabilization process causing the formation of a more-defined pore structure. It must be recognized that any polymer with high decomposition and chain rigidity can be a substitute candidate for Nafion to create high surface area porous CNFs. With this technique, the pore size can be easily tuned using process and solution parameters as will be shown below. We obtain extremely porous CNFs with a specific surface area of  $1600 \text{ m}^2 \text{ g}^{-1}$  and a high specific capacitance of  $210 \text{ F g}^{-1}$  by using a simple one-step carbonization process without the use of any activation procedure.

## 2. Experimental

### 2.1. Electrospinning process

Nafion powder (prepared by drying a LIQUION 1105 purchased from Ion Power Inc.) and PAN ( $M_w = 150,000 \text{ g mol}^{-1}$ , purchased from Sigma–Aldrich) were dissolved in DMF (purchased from Sigma–Aldrich) under gentle heating and stirring for 1 h. Fibers were electrospun at room temperature with humidity below 20%. The distance between the tip of the needle (22 gauge needle-spinneret from Hamilton Company) and the grounded collector was 5–6 inches, and the applied voltage of 8–10 kV was used to obtain a stable Taylor cone. The flow rate was kept at a constant  $0.5 \text{ mL h}^{-1}$ .

### 2.2. Carbonization process for fabrication of porous carbon nanofibers

The electrospun nanofibers were placed in a horizontal tube furnace and stabilized by heating to  $280^\circ\text{C}$  at a rate of  $5^\circ\text{C min}^{-1}$  under an air flow of  $200 \text{ mL min}^{-1}$ . The stabilized nanofibers were then carbonized by heating to  $700^\circ\text{C}$  at a rate of  $2^\circ\text{C min}^{-1}$  and held at  $700^\circ\text{C}$  for 1 h under an Argon flow of  $400 \text{ mL min}^{-1}$ . The carbonized fibers were then heated to  $800^\circ\text{C}$  and held for 1 h to further increase the conductivity. The complete decomposition of Nafion was confirmed by thermogravimetric analysis (Figure S.2). In addition, to elucidate the effect (if any) of Nafion decomposition on the electrodes, we conducted elemental analysis shown in Table S.1 of the supporting information. The carbonized Nafion: PAN and pure PAN nanofibers showed largely similar composition except for a small fraction of fluorine in the carbonized Nafion/PAN samples, possibly resulting from the Nafion backbone.

### 2.3. Nanofiber characterization

The external morphology of electrospun nanofiber mats was characterized using scanning electron microscopy (Zeiss Supra 50VP). To characterize internal assembly, nanofibers were embedded in epoxy matrix (purchased from Electron Microscopy Science) and then microtomed into thin longitudinal and cross-sections using a Leica EM UC6 ultramicrotome equipped with a diamond knife. The sections were picked up on lacey carbon copper grids

(purchased from Electron Microscopy Science) and characterized using transmission electron microscopy (JEOL JEM2100) operated at 200 kV. The specific surface area (SSA) of CNFs was measured using nitrogen sorption isotherms at 77 K (Autosorb-1, Quantachrome) and CO<sub>2</sub> sorption isotherms at 273 K (ASAP 2020, Micromeritics). Prior to the adsorption–desorption measurement, all samples were degassed at 200 °C under vacuum for 24 h to remove impurities. The pore size distribution (PSD) of CNFs was calculated based on adsorption–desorption curves using the quenched solid density functional theory (QSDFT) with assuming slit-shaped pores. The conductivity of CNFs was measured using a two-point method with stainless steel current collectors. Toray carbon paper with a known conductivity of 11 S cm<sup>−1</sup> was used to determine the contact and circuit resistance. The electrical conductivity,  $\sigma$ , was calculated by the formula:

$$\sigma = \frac{L}{R \times A} \quad (1)$$

where  $L$  is the electrode thickness,  $R$  is the resistance subtracted from the contact and circuit resistance, and  $A$  is the electrode area.

#### 2.4. Electrochemical capacitor performance

A symmetrical two-electrode cell was assembled using two pieces of fabricated CNFs with diameters of 3/8th inch and thicknesses in a range of 100–150 microns. The two electrodes were placed on either side of a Celgard 3501 separator and

sandwiched between two graphite current collectors (with negligible capacitance) (Figure S.5). The cell was housed inside two Teflon pieces pressed with screws and a clamp, and tested in 1 M H<sub>2</sub>SO<sub>4</sub>. Cyclic voltammetry was performed with various scan rates from 20 mV s<sup>−1</sup> to 5 V s<sup>−1</sup> in the voltage window from 0 to 0.9 V. Galvanostatic charge/discharge was carried out at different current densities from 1 A g<sup>−1</sup> to 20 A g<sup>−1</sup> within 0.9 V voltage window. The specific capacitance,  $C$ , was calculated by the following equation:

$$C = 4 * I * \Delta t / (m * \Delta V) \quad (2)$$

where  $I$  is the current (A),  $\Delta t$  is the discharging time (s),  $m$  is the total mass of CNFs (g), and  $\Delta V$  is the voltage window (V). The energy densities,  $E$  (Wh kg<sup>−1</sup>), were evaluated as a function of constant discharge power densities from 0.1 kW kg<sup>−1</sup> to 20 kW kg<sup>−1</sup> by the following equation:

$$E = \int (I * V * dt) / (3.6 * m) \quad (3)$$

where all variables are defined as earlier. Electrochemical impedance spectroscopy (EIS) was measured in the frequency range from 100 kHz to 20 mHz with an alternating current amplitude of 10 mV at open circuit voltage. All electrochemical measurements were carried out with potentiostat Gamry Reference 3000.

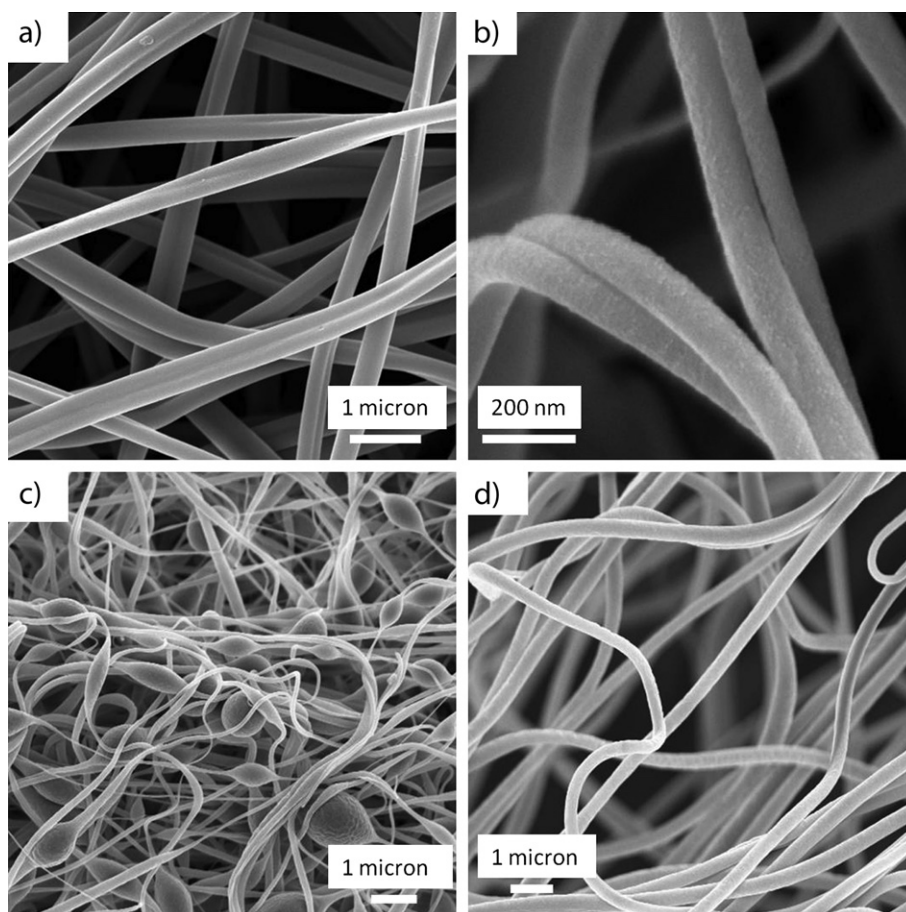


**Fig. 1.** SEM micrographs of electrospun PAN/Nafion nanofiber mats: (a) pure PAN with 10% total solid in DMF, (b) 60:40 Nafion:PAN with 15% total solid in DMF, (c) 80:20 Nafion:PAN with 20% total solid in DMF, (d) 80:20 Nafion:PAN with 25% total solid in DMF.

### 3. Results and discussion

The solutions of Nafion/polyacrylonitrile (PAN) in DMF were electrospun over a range of different mass ratios (Fig. 1). As Nafion: PAN weight ratio was increased, an increase in the total solid concentration in DMF was required to obtain smooth and bead-free nanofiber mats. For example, as shown in Fig. 1 and 60:40 (wt:wt) Nafion: PAN forms smooth nanofibers with a total solid concentration of 15 wt% in DMF. However, when the blend composition was changed to 80:20 (wt:wt) Nafion: PAN, bead-on-fiber morphology (Fig. 1c) was observed even at a 20 wt% total solid concentration in DMF. Uniform nanofibers (Fig. 1d) were obtained on increasing the total solid concentration to 25 wt%. This effect is attributed to the presence of Nafion aggregates in the solution (owing to electrostatic interactions) that lead to decrease in chain entanglement and loss of extensional viscosity [24]. Therefore, an increase in the total solid concentration is required to compensate for the increasing Nafion content. Our previous paper [24] provides a detailed study of morphology of electrospun Nafion/PAN nanofibers at different compositions and total solid concentrations in DMF.

To fabricate porous carbon nanofibers (CNFs), the blend nanofibers were subjected to oxidative carbonization procedures described in the Experimental methods section. During the oxidative stabilization step (at 280 °C), no pore formation was seen in any sample (Figure S.1) indicating that the Nafion was largely intact during the stabilization step. The high onset decomposition temperature of about 380 °C and excellent rigidity of Nafion [25] allowed the Nafion domain to retain its structural integrity while

the PAN domain underwent complex chemical reactions to transform into the stabilized ladder structure [26]. We believed and hypothesized that this property of the sacrificial polymer is critical because premature degradation of the sacrificial polymer before PAN stabilization (at 280 °C) will lead to closing up of the newly-developed pores. This hypothesis can possibly explain the lack of clear porosity, and modest increase in surface area in earlier works that utilized binary blends of PAN and a sacrificial polymer (different from Nafion) [18,20]. As expected, based on our hypothesis, prominent porous carbon structures (Fig. 2) appeared after heating to 800 °C under inert atmosphere due to selective removal of Nafion and conversion of PAN to carbon. When the Nafion: PAN weight ratio was 60:40, small crack-like pores were seen on fiber surfaces in SEM images (Fig. 2a). However, the TEM images of both longitudinal section and cross-section of the same sample (Fig. 3) showed a clear internal porous structure. The pores are interconnected within the carbon domains. As the Nafion content in the precursor was increased from 60% to 80%, the pores became bigger. Nevertheless, the fibers still retained their overall morphology after carbonization.

Note that the densities of Nafion and PAN are 1.7 and 1.2 g mL<sup>-1</sup> respectively; therefore the volume ratio of Nafion: PAN in the 80:20 wt:wt sample is ~75:25. It is very interesting how even at only 25 vol.% PAN, the Nafion: PAN CNFs did not collapse after selective removal of Nafion during carbonization and showed a uniform porous structure (Fig. 2b). The following two factors may have partially contributed to this effect. First, Nafion after drying at 80 °C for 24 h was still absorbing more than 10% water by weight [27] (as

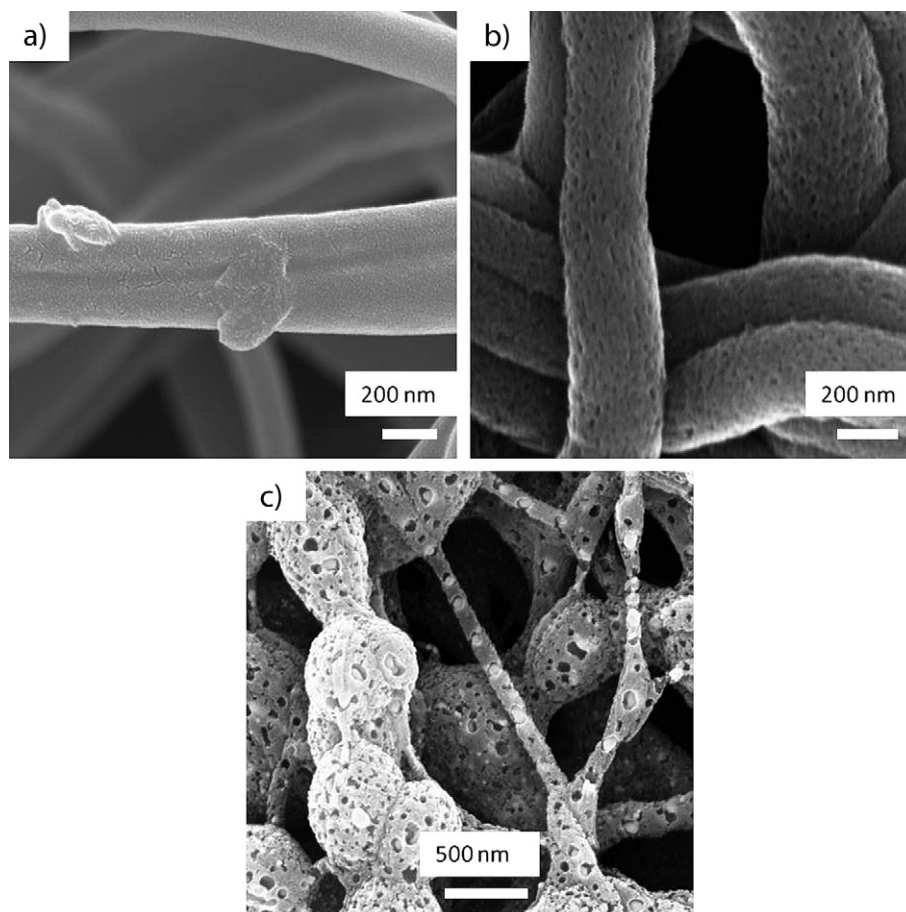


**Fig. 2.** SEM micrographs of porous carbon nanofibers formed by carbonizing nanofibers at different Nafion: PAN blend compositions: (a) 60:40 electrospun at 15% total solid concentration, (b) 80:20 electrospun at 25% total solid concentration, (c) 80:20 electrospun at 20% total solid concentration.

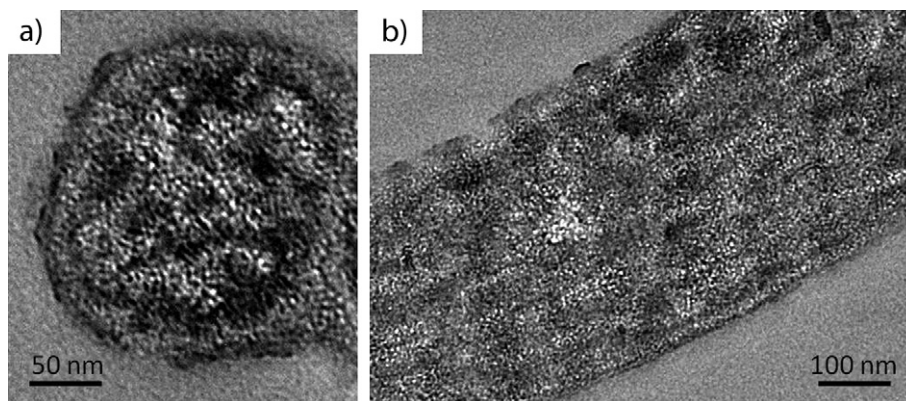


Fig. 3. TEM micrographs of microtomed sections of porous carbon nanofibers: (a and b) cross-section and longitudinal section of fibers of carbonized 60:40 Nafion: PAN.

confirmed by TGA in Figure S.2), which implied that the dry Nafion volume fraction was slightly lower than the calculated 75%. Secondly, the fiber diameter decreased from 250 nm to 200 nm after carbonization. A rough calculation will yield carbonized fibers with a volumetric ratio of 45:55 of solid carbon: intra-fiber pores. With 45% carbon, it is reasonable that the fibers still retain the shape after carbonizing 80:20 Nafion: PAN sample. Nevertheless, the retention of fiber morphology after carbonization and the presence of interconnected pore structure as seen in the TEM images implies that the PAN in the as-made nanofibers exhibits a continuous percolating domain, which when converted to carbon prevented the fiber from collapsing. We believe that the fast solvent evaporation and short residence time during electrospinning prevents complete phase separation of PAN and Nafion and kinetically traps the materials into a co-continuous assembly within nanofibers. Please refer to our recent paper that presented the TEM analysis of internal as-made nanofiber structures showing co-continuous assembly of PAN and Nafion [24]. Fig. 2b and c shows the effect of initial solution concentration on pore sizes after carbonization. Here both samples were electrospun using 80:20 weight ratio of PAN: Nafion, but the initial concentration of the solid in DMF was 25 and 20% respectively. As we decreased the solution concentration, the pore size after carbonization increased. We believe that the relaxation time of polymers during electrospinning for the sample with low solution concentration is shorter compared to those with high solution concentration. As a result, the domains of microphase separation are larger for the sample with shorter relaxation time, which leads to bigger pore size upon carbonization.

The pore size distribution (PSD), specific surface area, and pore volumes of porous CNFs were studied with the nitrogen adsorption–desorption isotherms (Fig. 4). The volume of adsorbed nitrogen of carbonized 80:20 Nafion: PAN increased slowly with relative pressure indicating the presence of a significant fraction of mesopores. On the other hand, the carbonized 60:40 Nafion: PAN was seen to level off at an intermediate pressure indicating the presence of a majority of micropores with a small amount of mesopores. Given that the desorption branch lies above the absorption branch, both hysteresis loops, obtained for carbonized 60:40 Nafion: PAN and 80:20 Nafion: PAN are associated with slit-shaped pores [28]. A summary of calculated BET surface area, total pore volume, volume of micropores, and average pore size from isotherms is listed in Table 1. The average pore size increased from 1.35 to 4.69 nm with increase of Nafion content from 60% to 80%. This is understandable as more sacrificial polymers are removed to create bigger pores. However, in spite of the increase in pore size, we did not see any significant decrease in surface area ( $1614 \text{ m}^2 \text{ g}^{-1}$  for 60% Nafion to  $1499 \text{ m}^2 \text{ g}^{-1}$  for 80% Nafion), which could be attributed to a significant increase in the overall pore volume in the carbonized 80:20 Nafion: PAN ( $1.336 \text{ cm}^3 \text{ g}^{-1}$ ) compared to carbonized 60:40 Nafion: PAN ( $0.822 \text{ cm}^3 \text{ g}^{-1}$ ). Kim et al. [19] obtained  $237 \text{ m}^2 \text{ g}^{-1}$  for carbonized pure PAN, while other researchers [22] obtained up to  $550 \text{ m}^2 \text{ g}^{-1}$  for blends of PAN with polyvinylpyrrolone. It is obvious that the use of Nafion as a sacrificial polymer allowed us to fabricate porous CNFs with a surface area three times higher than previous works. Even though the pore size distributions are broad (Figure S.3), the benefit of adjustable pore size and high specific surface area

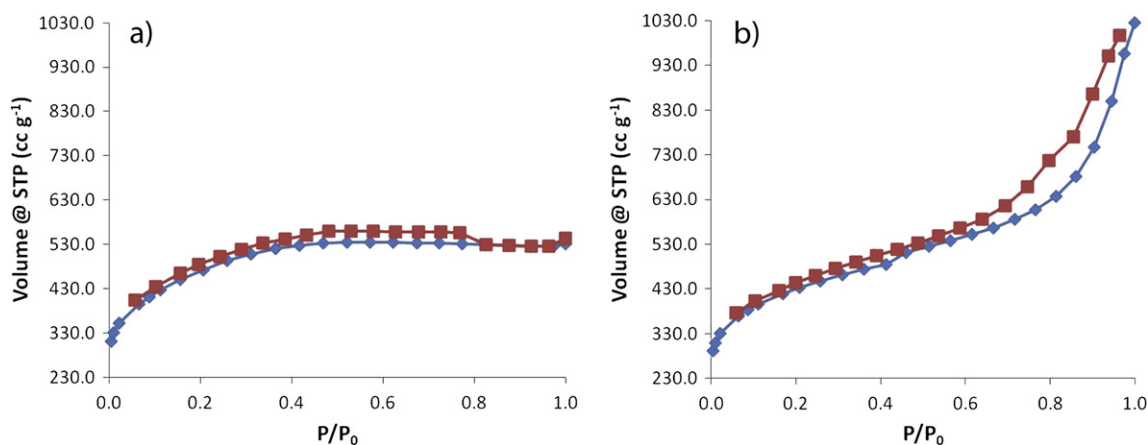


Fig. 4. Nitrogen sorption isotherms of carbonized (a) 60:40 Nafion: PAN and (b) 80:20 Nafion: PAN.

**Table 1**Values of SSA, pore volume, average pore size acquired from N<sub>2</sub> sorption.

	BET SSA (m <sup>2</sup> g <sup>-1</sup> )	V <sub>micro</sub> (cm <sup>3</sup> g <sup>-1</sup> )	V <sub>meso</sub> (cm <sup>3</sup> g <sup>-1</sup> )	Cumulative pore volume (cm <sup>3</sup> g <sup>-1</sup> )	Average pore size (nm)
Nafion:PAN 60:40	1614	0.641	0.181	0.822	1.35
Nafion:PAN 80:20	1499	0.526	0.810	1.336	4.69
PAN	339	0.128	–	0.128	0.6

(SSA) is extremely attractive for the study in supercapacitors. In addition, the presence of interconnected pores as seen in TEM study in Fig. 3, we believe, will be extremely beneficial in supercapacitor applications owing to greater electrolyte accessibility.

To study the performance of nanofiber mats as electrodes in supercapacitors, resulting porous CNFs were punched into circular-shaped mats with diameters of 3/8th inch with thicknesses in a range of 100–150 microns and used as free-standing electrodes as-is without the addition of any binder or conductive material. Note that thick electrodes can potentially increase electrolyte diffusion resistance and electrical resistance within electrodes and therefore deteriorate the F g<sup>-1</sup> or F cm<sup>-3</sup> performance. However, from our experiments we find that this deterioration effect is seen only for electrodes thicker than 200 microns since the CNFs showed a very good hydrophilicity as investigated by contact angle measurements shown in the supporting information (Figure S.8). We found that the use of graphite as the current collector allowed us to achieve a lower resistance due to improved contact between the electrode and the current collector which is indicated by the

x-intercept of Nyquist plot at high frequencies (Figure S.4). Fig. 5a and b shows the cyclic voltammograms of carbonized 60:40 and 80:20 Nafion:PAN samples at various voltage scan rates. Both carbonized 60:40 Nafion:PAN and 80:20 Nafion:PAN exhibit near-rectangular cyclic voltammetry curves at both slow and fast scan rates indicating a fast charge/discharge behavior and a low resistance of materials. The use of free-standing porous CNFs (without any binders) with pore sizes larger than the solvated ion size (~1 nm) in the electrolyte allowed us to achieve such kind of high power handling capability. While the carbonized 80:20 Nafion:PAN maintained near-rectangular ideal CV shape up to a high scan rate of 2 V s<sup>-1</sup>, the carbonized 60:40 Nafion:PAN could operate up to 1 V s<sup>-1</sup> with near-ideal behavior. The relatively higher power handling capability (i.e. faster ion transport) of carbonized 80:20 Nafion:PAN than carbonized 60:40 is possibly due to the larger pore sizes in carbonized 80:20 Nafion:PAN nanofibers. This is very promising as activated carbon with SSA of 2500 m<sup>2</sup> g<sup>-1</sup> showed deviation from an ideal rectangular shape at only 100 mV s<sup>-1</sup> scan rate in 0.5 M K<sub>2</sub>SO<sub>4</sub> [29]. At a scan rate of 20 mV s<sup>-1</sup>, carbonized 60:40 Nafion:PAN and 80:20 Nafion:PAN exhibit large volumetric capacitances of 53 and 60 F cm<sup>-3</sup> respectively in spite of the relatively low packing density of electrospun nanofiber mats (see Fig. 5c) [30]. Further improvement of packing density and hence the volumetric capacitance can be made by hot pressing before carbonization, and this work is currently underway [31]. Note that both materials show a similar trend of specific capacitance vs. scan rate (Fig. 5c) with no clear difference in spite of different pore sizes. This will be discussed further below along with the results of Fig. 7.

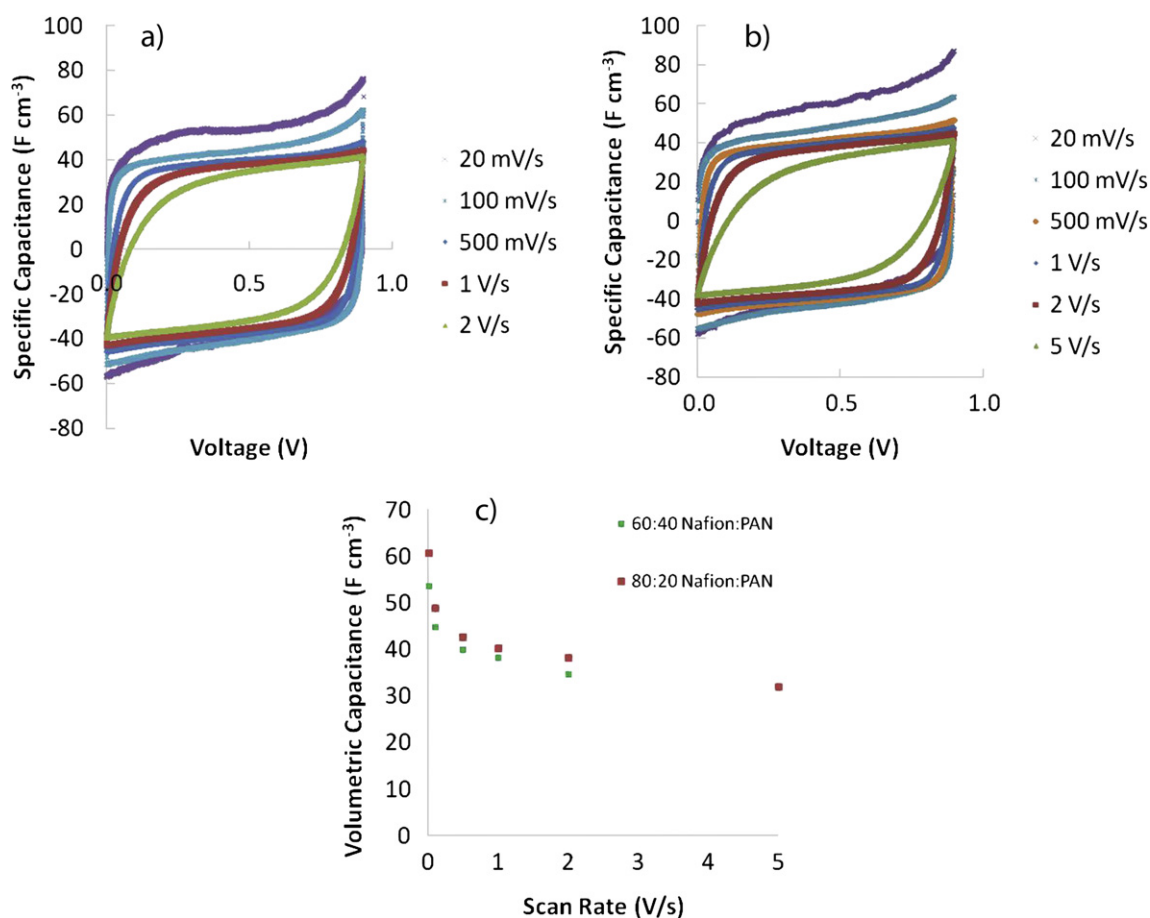


**Fig. 5.** Cyclic voltammetry (CV) of (a) carbonized 60:40 Nafion:PAN and (b) carbonized 80:20 Nafion:PAN; and (c) the resulted volumetric capacitance at different scan rates.

Table 2 shows the electronic conductivity and gravimetric specific capacitance measured via charge–discharge experiments for three different carbonized samples with the following initial Nafion: PAN weight ratio; 0:100 (pure PAN), 60:40 and 80:20. As expected, the conductivity reduced as the pore volume increased from  $0.15 \text{ S cm}^{-1}$  in carbonized pure PAN to  $0.12 \text{ S cm}^{-1}$  in carbonized 80:20 Nafion: PAN nanofibers. The small reduction in conductivity was due to the fact that porous CNFs still remained intact with a continuous carbon phase upon removing Nafion. Although by increasing the carbonization temperature from 800 to  $1000^\circ\text{C}$ , the conductivity of carbonized pure PAN could be increased to  $2.3 \text{ S cm}^{-1}$  but the capacitance decreased from  $20 \text{ F g}^{-1}$  to  $15 \text{ F g}^{-1}$ . These values are comparable to the result recently obtained by Zhi et al. [32]. They reported a conductivity of  $1.25 \text{ S cm}^{-1}$  and a specific capacitance of  $10 \text{ F g}^{-1}$  (in  $1 \text{ M Na}_2\text{SO}_4$ ) for carbonized electrospun PAN at  $850^\circ\text{C}$ . As shown in Table 2, the gravimetric specific capacitances measured via charge–discharge experiments at a current density of  $1 \text{ A g}^{-1}$  were 190 and  $210 \text{ F g}^{-1}$  for carbonized 60:40 Nafion: PAN and 80:20 Nafion: PAN respectively. These values corroborated the advantage of pores within individual nanofibers. For comparison, specific capacitance of activated CNFs fabricated using an additional high temperature activation procedure after carbonization has been reported to be up to  $180 \text{ F g}^{-1}$  at the same discharge current density [15,33]. The use of sacrificial Nafion to create porous CNFs not only allowed a one-step fabrication process, but also allowed us to further improve the performance compared to activated CNFs.

Note that although 80:20 Nafion: PAN sample had a slightly smaller surface area and lower conductivity than 60:40 Nafion: PAN, its gravimetric and volumetric capacitance was higher than 60:40 Nafion: PAN. The bigger pore size of 80:20 Nafion: PAN allowed enhanced ion diffusion and provided more accessible carbon surface area leading to improved performance. Chmiola [34] studied the effect of pore size on the performance of supercapacitor by using carbide-derived carbon, and showed a decrease of normalized capacitance when the pore size was reduced to  $\sim 1 \text{ nm}$ . We observed a similar trend with our materials. Note that in this study we used aqueous  $\text{H}_2\text{SO}_4$  as the electrolyte that consisted of solvated ions of size  $\sim 1 \text{ nm}$ ; therefore both our porous nanofiber samples provided pore sizes large enough for ion diffusion and improved surface accessibility and hence the increase of the specific capacitance in 80:20 Nafion: PAN sample was not as drastic. Ability to increase pore size and yet maintain a high specific surface area, will be particularly beneficial with organic electrolytes that typically

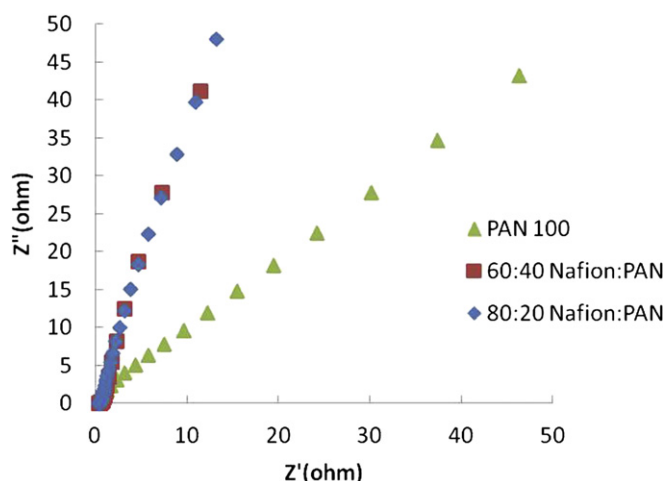


Fig. 6. Nyquist plots of different carbonized samples.

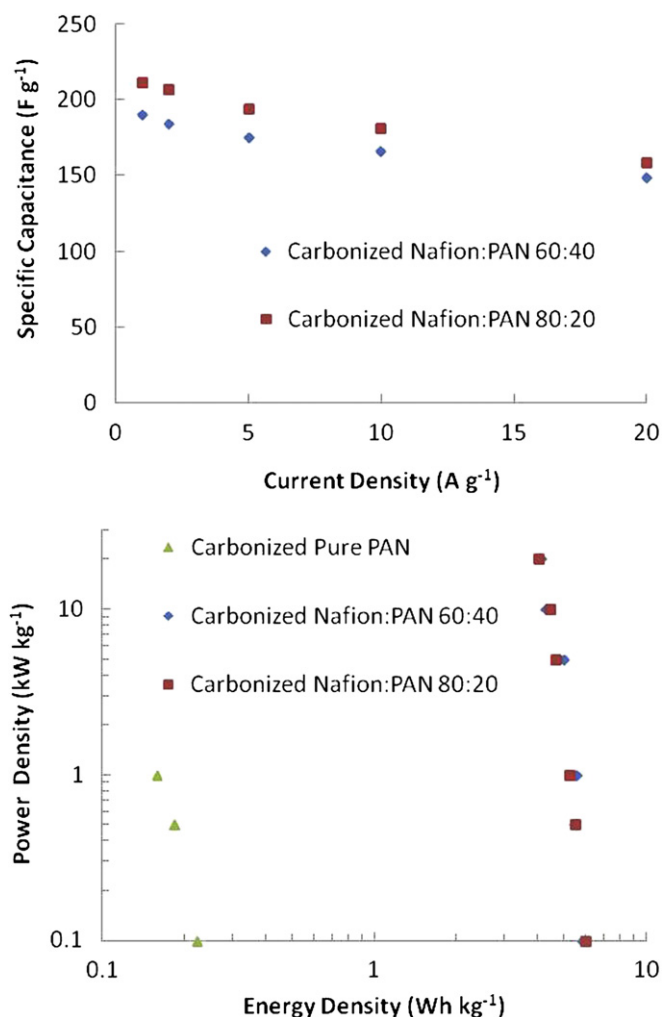


Fig. 7. Specific capacitance versus current density (top) and Ragone plots of different carbonized samples (bottom).

have larger solvated ion sizes than aqueous solutions. Use of organic electrolytes is critical for most industrial applications as they allow capacitor to operate at much higher voltages (up to  $3 \text{ V}$ ) than aqueous electrolytes ( $1 \text{ V}$ ). Therefore, it allows improved energy density, which is proportional to  $V^2$ . Study on effect of pore size in organic electrolytes is currently underway. Fig. 6 shows the AC impedance measurements of porous CNFs. The Nyquist plots of carbonized 60:40 Nafion: PAN and 80:20 Nafion: PAN showed small depressed arcs at high frequencies and steep linear slopes at low frequencies. We conducted the same experiment on carbonized pure PAN (non-porous carbon nanofiber mat) as reference, which showed a gentle  $45^\circ$  slope at low frequencies. This indicates that both porous nanofiber samples possess a small charge transfer resistance and fast kinetics of ion adsorption to the electrode.

Table 2  
Values of conductivity and gravimetric capacitance of different carbonized samples.

	Conductivity ( $\text{S cm}^{-1}$ )	Specific capacitance ( $\text{F g}^{-1}$ ) at $1 \text{ A g}^{-1}$
Nafion: PAN 0:100 <sup>a</sup>	0.15	20
Nafion: PAN 0:100 <sup>b</sup>	2.3	15
Nafion: PAN 60:40 <sup>a</sup>	0.13	190
Nafion: PAN 80:20 <sup>a</sup>	0.12	210

<sup>a</sup> The samples were carbonized at  $800^\circ\text{C}$ .

<sup>b</sup> The sample was carbonized at  $1000^\circ\text{C}$ .

Finally, specific capacitance versus current density plots and Ragone plots were constructed by varying the discharging current density from  $1 \text{ A g}^{-1}$  to  $20 \text{ A g}^{-1}$  and power density from  $0.1 \text{ kW kg}^{-1}$  to  $20 \text{ kW kg}^{-1}$  respectively (Fig. 7). A similar trend of reduction of specific capacitance was observed for both carbonized samples. Interestingly, only  $\sim 25\%$  reduction of specific capacitance was seen upon increasing the current density from  $1 \text{ A g}^{-1}$  to  $20 \text{ A g}^{-1}$ . Activated carbons have been shown to lose more than  $50\%$  of their capacitance at a current density of  $20 \text{ A g}^{-1}$  [15]. As a result, Ragone plots showed a very small reduction in energy density upon increasing power density for both carbonized samples with Nafion, i.e. porous carbon nanofibers. This behavior is often associated with fast kinetics of ion diffusion and adsorption to the electrode surface which is related to structural advantages as described earlier. We achieved an energy density of  $4 \text{ Wh kg}^{-1}$  at a power density of  $20 \text{ kW kg}^{-1}$ . It must be noted that these values are evaluated based on the mass of two electrodes and the voltage of the cell without including the mass of the current collectors, separator, and the electrolytes. As mentioned earlier, the difference in the power handling capability between the two porous carbon nanofiber samples, as determined from capacitance vs. scan rate/current density and Ragone plots is not significant as both provide large enough pores for transport of solvated ions in the aqueous electrolyte.

#### 4. Conclusion

In summary, we have demonstrated the fabrication of highly porous, high surface area carbon nanofibers (CNFs) by electrospinning a blend of polyacrylonitrile (PAN) and Nafion followed by high temperature carbonization. The high decomposition temperature of Nafion prevented its premature degradation before PAN stabilization and allowed the formation of well-defined pore structure upon complete carbonization of PAN and selective decomposition of Nafion. It must be recognized that any polymer with high decomposition temperature and chain rigidity can be a substitute candidate for Nafion to create high surface area porous CNFs. In addition, tunability of pore size within nanofibers was demonstrated with the use of different blend compositions. These materials possess an excellent performance with a specific capacitance of greater  $200 \text{ F g}^{-1}$  at relatively high rate capability when applied as free-standing electrodes for supercapacitors. This is attributed to the large surface area and large fraction of mesopores that allows improved electrode surface accessibility. The materials exhibit near-ideal capacitive behavior at both low and fast scan rates ( $2 \text{ V s}^{-1}$ ) during cyclic voltammetry study. In addition, on increasing the current density from  $1 \text{ A g}^{-1}$  to  $20 \text{ A g}^{-1}$ , they retain  $75\%$  of their capacitance indicating fast charge–discharge rates and high power handling capability. This is attributed to the presence of a hierarchical pore structure in these carbon electrodes, which allows us to enhance both surface area and ion transport.

#### Acknowledgements

The authors would like to acknowledge National Science Foundation (Grant Numbers 1150528 and 1236466) for financial support. The authors also would like to thank Prof. Yossef Elabd, Prof. Giuseppe Palmese and their group members for access to their lab equipment during preliminary experiments. The authors are

grateful to Prof. Yuri Gogotsi and his group for BET surface area measurements and the Centralized Research Facility of Drexel University for instrumentation support.

#### Appendix A. Supplementary data

Supplementary data related to this article can be found at <http://dx.doi.org/10.1016/j.jpowsour.2013.01.080>.

#### References

- [1] A.G. Pandolfo, A.F. Hollenkamp, *Journal of Power Sources* 157 (2006) 11–27.
- [2] O. Barbieri, M. Hahn, A. Herzog, R. Kotz, *Carbon* 43 (2005) 1303–1310.
- [3] T. Morimoto, K. Hiratsuka, Y. Sanda, K. Kurihara, *Journal of Power Sources* 60 (1996) 239.
- [4] M. Bledamartinez, J. Maciaagullo, D. Lozanocastello, E. Morallon, D. Cazorlaamoros, A. Linaresolano, *Carbon* 43 (2005) 2677–2684.
- [5] Y. Gogotsi, A. Nikitin, H. Ye, W. Zhou, J.E. Fischer, B. Yi, H.C. Foley, M.W. Barsoum, *Nature Materials* 2 (2003) 591–594.
- [6] C. Portet, J. Chmiola, Y. Gogotsi, S. Park, K. Lian, *Electrochimica Acta* 53 (2008) 7675–7680.
- [7] E. Frackowiak, K. Metenier, V. Bertagna, F. Beguin, *Applied Physics Letters* 77 (2000) 2421.
- [8] D. Carriazo, F. Picó, M.C. Gutiérrez, F. Rubio, J.M. Rojo, F. del Monte, *Journal of Materials Chemistry* 20 (2010) 773.
- [9] J. Li, X. Wang, Q. Huang, S. Gamboa, P.J. Sebastian, *Journal of Power Sources* 158 (2006) 784–788.
- [10] C. Vixguterl, E. Frackowiak, K. Jurewicz, M. Friebe, J. Parmentier, F. Beguin, *Carbon* 43 (2005) 1293–1302.
- [11] C. Kim, K.-S. Yang, W.-J. Lee, *Electrochemical and Solid-State Letters* 7 (2004) A397.
- [12] C. Kim, S. Park, W. Lee, K. Yang, *Electrochimica Acta* 50 (2004) 877–881.
- [13] Z. Tai, X. Yan, J. Lang, Q. Xue, *Journal of Power Sources* 199 (2012) 373–378.
- [14] Q. Guo, X. Zhou, X. Li, S. Chen, A. Seema, A. Greiner, H. Hou, *Journal of Materials Chemistry* 19 (2009) 2810.
- [15] E.J. Ra, E. Raymundo-Piñero, Y.H. Lee, F. Béguin, *Carbon* 47 (2009) 2984–2992.
- [16] B. Xu, F. Wu, R. Chen, G. Cao, S. Chen, Y. Yang, *Journal of Power Sources* 195 (2010) 2118–2124.
- [17] L.L. Zhang, X.S. Zhao, *Chemical Society Reviews* 38 (2009) 2520.
- [18] L. Ji, A.J. Medford, X. Zhang, *Journal of Polymer Science Part B: Polymer Physics* 47 (2009) 493–503.
- [19] B.-H. Kim, K.S. Yang, H.-G. Woo, K. Oshida, *Synthetic Metals* 161 (2011) 1211–1216.
- [20] L. Zhang, Y.-L. Hsieh, *European Polymer Journal* 45 (2009) 47–56.
- [21] C. Kim, Y.I. Jeong, B.T.N. Ngoc, K.S. Yang, M. Kojima, Y.A. Kim, M. Endo, J.-W. Lee, *Small* 3 (2007) 91–95.
- [22] H. Niu, J. Zhang, Z. Xie, X. Wang, T. Lin, *Carbon* 49 (2011) 2380–2388.
- [23] C. Kim, B.T.N. Ngoc, K.S. Yang, M. Kojima, Y.A. Kim, Y.J. Kim, M. Endo, S.C. Yang, *Advanced Materials* 19 (2007) 2341–2346.
- [24] C. Tran, V. Kalra, *Soft Matter* (2012). <http://dx.doi.org/10.1039/c1032sm25976a>.
- [25] C. Wikie, J. Thomsen, M. Mittleman, *Journal of Applied Polymer Science* 42 (1991) 901.
- [26] T. Sun, Y. Hou, H. Wang, *Journal of Applied Polymer Science* 118 (2010) 462–468.
- [27] C.-H. Ma, T.L. Yu, H.-L. Lin, Y.-T. Huang, Y.-L. Chen, U.S. Jeng, Y.-H. Lai, Y.-S. Sun, *Polymer* 50 (2009) 1764–1777.
- [28] M. Peng, D. Li, L. Shen, Y. Chen, Q. Zheng, H. Wang, *Langmuir* 22 (2006) 9368–9374.
- [29] R. Lin, P.L. Taberna, J. Chmiola, D. Guay, Y. Gogotsi, P. Simon, *Journal of the Electrochemical Society* 156 (2009) A7.
- [30] V. Presser, L. Zhang, J.J. Niu, J. McDonough, C. Perez, H. Fong, Y. Gogotsi, *Advanced Energy Materials* 1 (2011) 423–430.
- [31] Y. Yang, F. Simeon, T.A. Hatton, G.C. Rutledge, *Journal of Applied Polymer Science* 124 (2012) 3861–3870.
- [32] M. Zhi, A. Manivannan, F. Meng, N. Wu, *Journal of Power Sources* 208 (2012) 345–353.
- [33] C. Kim, K.S. Yang, *Applied Physics Letters* 83 (2003) 1216.
- [34] J. Chmiola, *Science* 313 (2006) 1760–1763.